Temperature dependent carrier mobility in organic field-effect transistors: The role of dielectrics (9)

Cite as: J. Appl. Phys. 125, 035501 (2019); https://doi.org/10.1063/1.5064809 Submitted: 08 October 2018 . Accepted: 01 January 2019 . Published Online: 16 January 2019

A. Laudari 📵, and S. Guha 📵

COLLECTIONS

EP

This paper was selected as an Editor's Pick







ARTICLES YOU MAY BE INTERESTED IN

Mitigating wakeup effect and improving endurance of ferroelectric HfO₂-ZrO₂ thin films by careful La-doping

Journal of Applied Physics 125, 034101 (2019); https://doi.org/10.1063/1.5050700

Strain and property tuning of the 3D framed epitaxial nanocomposite thin films via interlayer thickness variation

Journal of Applied Physics 125, 082530 (2019); https://doi.org/10.1063/1.5053705

Time-dependent characteristics of secondary electron emission

Journal of Applied Physics 125, 024902 (2019); https://doi.org/10.1063/1.5080264





Temperature dependent carrier mobility in organic field-effect transistors: The role of dielectrics

Cite as: J. Appl. Phys. 125, 035501 (2019); doi: 10.1063/1.5064809

Submitted: 8 October 2018 · Accepted: 1 January 2019 ·

Published Online: 16 January 2019







A. Laudari and S. Guha De

AFFILIATIONS

Department of Physics and Astronomy, University of Missouri, Columbia, Missouri 65211, USA

a)Electronic mail: guhas@missouri.edu

ABSTRACT

It has been shown that the use of a ferroelectric dielectric in 6,13-bis(triisopropylsilylethynyl)pentacene (TIPS-pentacene) field-effect transistors (FETs) results in a negative coefficient of carrier mobility, a signature of a band-like transport, above a certain temperature [A. Laudari and S. Guha, Phys. Rev. Appl. 6, 044007 (2016)]. Along with spontaneous polarization, polymer ferroelectric dielectrics offer a platform for tuning interfacial transport in FETs as their dielectric constant may vary nearly by an order of magnitude with temperature. In this work, we explore a variety of organic and inorganic dielectrics with varying dielectric constants on the temperature-dependent transport properties of TIPS-pentacene organic FETs to obtain a comprehensive insight into the role of energetic disorder and trap states. In particular, a high κ dielectric, Al_2O_3 , shows an activated transport throughout the temperature regime, whereas the ferroelectric copolymer poly(vinylidene fluoride-co-trifluoroethylene) (PVDF-TrFE), with comparable and even higher values of κ compared to Al_2O_3 , above 200 K shows a very different behavior. Additionally, the external poling condition of the PVDF-TrFE dielectric plays a role. We attribute the band-like negative coefficient of carrier mobility, observed at high temperatures, in TIPS-pentacene FETs with unpoled PVDF-TrFE to a polarization fluctuation process and explore this phenomenon using the concept of transport energy.

Published under license by AIP Publishing. https://doi.org/10.1063/1.5064809

I. INTRODUCTION

Invoking concepts from amorphous semiconductors, disordered systems, in general, are characterized by both extended and localized states where the transport of carriers typically occurs through the exponential tail states. The presence of grain boundaries and molecular-level disorder results in localized states; hopping of carriers within these states gives rise to the mechanism of conduction. In the absence of a long-range order as in amorphous materials, the sharp features seen in the density of states (DOS) of crystalline materials disappear. The concept of a mobility edge, which plays the same role as band edges in a crystal, is often used in disordered systems to discuss transport [see Fig. 1(a)]. In addition to localized defect states near the Fermi energy (E_F), disorder-induced DOS band tails are present up to their mobility edge in amorphous semiconductors. If the Fermi level is located in the region of localized states, the conductivity may arise either from thermal excitation of carriers across a mobility gap into extended states or by a hopping process. The former mechanism is the dominant process at high temperatures, and the latter dominates charge transport at lower temperatures.

The carrier mobility, μ , in crystalline silicon field-effect transistors (FETs) is scattering limited and is directly related to the conductivity (σ) by

$$\sigma = q\mu n,$$
 (1)

where q is the elementary charge and n is the carrier density. Equation (1) is valid as long as one neglects electron-electron interactions. Thus, if n is known in crystalline semiconductors, measurement of conductivity yields directly the field-effect μ . In disordered materials, a relationship between μ (field-effect) and σ is not straightforward since carriers are trapped and only those that can excite to the so-called "transport band," then contribute to σ . The general mechanism of transport in organic FETs consisting of molecular or polymeric semiconductors is usually discussed within the framework of hopping

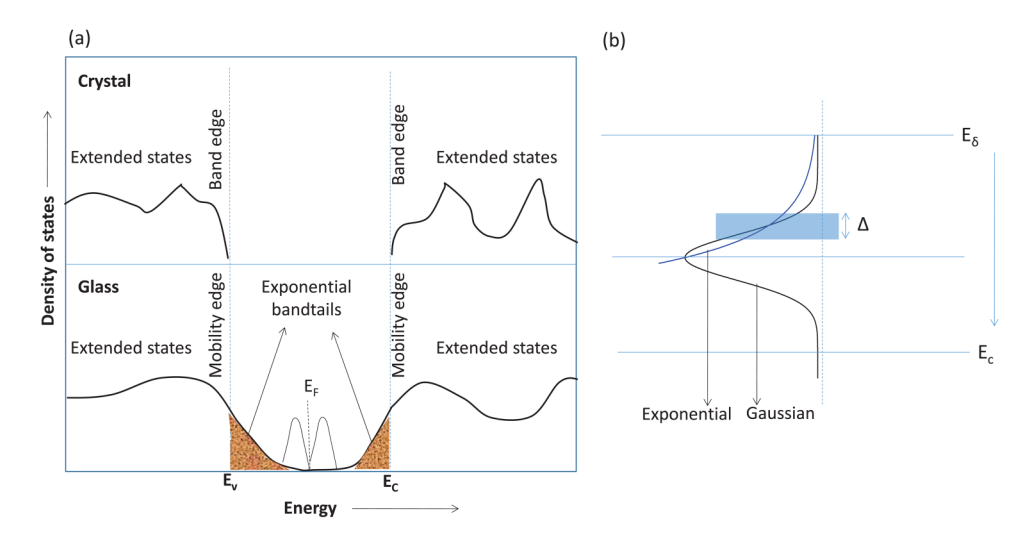


FIG. 1. (a) Schematic of DOS for a crystalline and an amorphous semiconductor. The mobility edges in an amorphous semiconductor play a similar role as the band edges in a crystal. (b) Comparison of Gaussian and exponential DOS. Energy is shown to increase downwards. Δ is the maximum energy interval sampled by the quasi-Fermi level.

between disordered-localized state and in terms of various polaronic models. ^{2,3} Additionally, there may be a dynamic coupling of charge carriers to the electronic polarization at the organic semiconductor-dielectric interface. ^{4,5} The formation of Fröhlich surface polarons has been further observed if the gate dielectric is sufficiently polar, ⁶ which manifests itself as reduced charge carrier mobility. A similar effect seen in metal oxide semiconductor FETs (MOSFETs), termed as "remote phonon scattering," is known to reduce the effective electron mobility in the inversion layer of the Si substrate, especially when high κ dielectrics are used. ^{7,8} The work by Servati et al. ⁹ recasts the FET mobility as $\mu_{\text{FET}} = \mu_{\text{eff}}\Theta$, where μ_{eff} , the physical mobility, represents temperature dependent hopping transport and Θ depends upon device parameters, responsible for the bias dependence of μ_{FET} .

Although organic semiconductors are weakly bonded (van der Waals) compared to covalently bonded inorganic semiconductors, it is possible to achieve a high degree of order by processing conditions of small molecule based thin films or by a self-assembly process in complex donor-acceptor polymers.¹⁰ As a result, the temperature dependence of carrier transport in organic semiconductors may show band transport, tunneling, or an activated process. 11 Highly ordered molecular crystals in FET architecture show an activated process with increasing μ_{FET} with temperature in the low temperature range, mainly due to impurities that act as traps and a band-like transport with a negative coefficient of μ_{FET} with temperature at higher temperatures. The high temperature regime is thus due to the lattice phonons. For transport to be described by a bandmodel: $\mu > er^2/2\hbar$, where r is the intermolecular distance, e is the electronic charge, and \hbar is Planck's constant. With typical values of r as 3-4 Å, the above condition translates to FET mobilities being greater than 1-2 cm²/Vs, ensuring the energy bandwidth to be larger than the energy change involved in scattering. Thus, for ordered organic semiconductors, a Drude-type transport is conceivable. Furthermore, it has also been shown that inhomogeneous strain at the semiconductor-dielectric interface due to mismatch between the coefficients of thermal expansion dictates the hopping nature versus band-like transport in organic FETs. 13

Ferroelectrics have the property of possessing macroscopic spontaneous polarization that can be re-oriented through the application of an external electric field. There has been a substantial amount of work in using the relaxor ferroelectric polymer: poly(vinylidene fluoride) (PVDF) and its copolymers such as PVDF-trifluoroethylene (PVDF-TrFE) as the gate dielectric layer in polymer based ferroelectric FETs for memory and other applications. 14-17 The ferroelectric phase occurs in the all-trans or β -phase of the polymer. ¹⁸ The copolymer, PVDF-TrFE, has the advantage of being ferroelectric directly after solution processing of the film, while PVDF requires additional measures such as stretching or controlled heating of the film to ensure all trans-configuration. 19 As with any ferroelectric material, the dielectric constant (κ) of PVDF-TrFE increases almost by a factor of five until its ferroelectric-paraelectric transition temperature at 390 K. By using the same organic semiconductor-insulator interface, ferroelectric dielectrics, thus, allow a platform for tuning the polarization strength with temperature. Also, PVDF-TrFE as a dielectric in organic FETs emphasizes polarization fluctuation dominant transport.20

It was observed that 6,13-bis(triiso-propylsilylethynyl) pentacene (TIPS-pentacene) based FETs show a hopping transport as a function of temperature (T) with $d\mu/dT > 0$ or a band-like transport with $d\mu/dT < 0$, depending on the choice of the dielectric.²¹ Even with carrier mobilities lower

than what is required to reach disorder-free limits (Drude-type), the choice of PVDF-TrFE clearly showed a reversible behavior in $\mu_{\rm FET}$ with T. A band-like transport was observed beyond 200 K, and this effect was not seen with non-ferroelectric dielectrics. In addition to polarization fluctuation, thermal lattice fluctuations may also play a role in FET transport, which could result in band-like transport. 22 A question that arises is whether it is explicitly the high κ of the gate insulator that plays a role in the different transport regime with temperature or does the polarization fluctuation, inherent to polymer ferroelectrics, result in $d\mu/dT < 0$? Furthermore, one may ask whether this is a universal phenomenon with ferroelectric dielectrics or whether the nature of the trap/localized states in TIPS-pentacene facilitates such a band-like transport.

Here, we compare temperature-dependent transport from TIPS-pentacene FETs using both non-ferroelectric and ferroelectric dielectrics. Specifically, the use of Al₂O₃ as a dielectric with comparable value of κ to PVDF-TrFE shows that the band-like transport observed with PVDF-TrFE is not just due to a strong dynamic coupling of the carriers at the interface but rather due to polarization fluctuation inherent to ferroelectric films. Additionally, poling the ferroelectric dielectric also affects the temperature-dependent behavior. External poling of the ferroelectric film (by applying an external electric field while heating the PVDF-TrFE film just above the ferroelectric-paraelectric transition temperature) has a distinct role in altering the semiconductor-insulator interface and thus impact transport properties in FETs. The subthreshold swing and carrier mobility of organic FETs are significantly improved by vertical poling, whereas lateral poling deteriorates the FET on/off ratio and, subsequently, the subthreshold swing.²³ Curiously, the temperature dependence of TIPS-pentacene FETs with vertically poled PVDF-TrFE films shows an activated transport throughout the temperature range of the measurements. It is mainly in the unpoled PVDF-TrFE film where polarization fluctuation plays a significant role, and it consequently shows a band-like behavior above 200 K in TIPS-pentacene FETs. Furthermore, bulk transport in TIPS-pentacene is dominated by shallow trapping with discrete traps. A combination of the nature of trap levels in the semiconductor and polarization fluctuation is responsible for a band-like transport in TIPS-pentacene FETs above a certain temperature. We explain the above on the basis of the so-called transport energy.

II. EXPERIMENTAL

A. Materials and device fabrication

6,13-Bis(triisopropylsilylethynyl)pentacene (TIPS-pentacene) was procured from Sigma Aldrich, Inc. and used without any purification. Poly(vinylidenefluoride-co trifluoroethylene) (PVDF-TrFE) (75/25) was obtained from Measurement Specialties, Inc., USA. Poly-4-vinyl phenol (PVP) with average molecular weight (Mw) 25 000 g/mol, propylene glycol monomethyl ether acetate (PGMEA) with Mw 132.16 g/mol, and cross-linking agent poly(melamine-coformaldehyde)

methylated 84% solution in 1 butane (PMMF) were procured from Sigma Aldrich, Inc. The solvents N,N-dimethylformamide (DMF) and anhydrous toluene were procured from Sigma Aldrich, Inc. CYTOP (CTL-809M) was bought from Asahi Glass Co. Ltd., Japan.

Bottom-gate top-contact and top-gate bottom-contact FETs were fabricated by evaporating 60 nm Al as gate and 50 nm gold as source and drain electrodes using a shadow mask. The PVDF-TrFE dielectric layer on Al coated glass substrates was obtained as described in a prior work. 24 Al $_2$ O $_3$ dielectric layer was grown using the atomic layer deposition method on p^{++} Si (100) wafers. 25 The TIPS-pentacene films were obtained through slow crystallization growth in a solvent-saturated atmosphere. 21 For top-gate bottom-contact FET, CYTOP was spincoated on top of TIPS-pentacene, followed by 60 nm aluminum as top gate. All fabrication steps except the growth of TIPS-pentacene films were carried out in a glovebox under the nitrogen atmosphere.

The vertical poling of the PVDF-TrFE film was carried out as described in Ref. 23. PVDF-TrFE was dissolved in DMF (50 mg/ml). This dielectric solution was then spin casted on top of the Al coated glass at a spin speed of 1600 rpm for 60 s and heated at 70 °C for 10 min to remove the solvent residue. The PVDF-TrFE film was vertically poled by applying an electric field of $\sim 100 \, \text{MV/m}$ during the crystallization process, i.e., while annealing the film at 135° for $1/2 \, \text{h}$. A temporary electrode was prepared by depositing 300 nm of Al on a glass slide. Electrical contacts were made and the slide was placed (with the Al strip facing down) on top of the PVDF-TrFE film. A 50 g weight was added on top to ensure a uniform contact of the top electrode with the ferroelectric surface. The field was applied between the temporary top electrode and the bottom Al electrode.

B. Device characterization

The capacitance measurements from MIS diodes were carried out with an HP 4284A precision LCR meter. During the measurement, a DC voltage is applied to the capacitor with a small AC voltage signal superimposed over the DC signal. Capacitance is recorded as the DC bias is swept. The magnitude of the AC signal was 200 mV, and the frequency of the signal was $5\,\mathrm{kHz}$ for all measurements. The DC signal was swept both from positive to negative bias and vice versa.

Room temperature DC electrical characterizations were performed using two source-meters, Keithley 2400 and Keithley 236, using a customized LabVIEW program. For temperature-dependent electrical measurements, a dual source-meter Keithley 2612B was used. The FETs were kept inside a closed-cycle helium cryostat (APD Cryogenics) where the temperature may be varied from 11 K to 480 K. The temperature was measured using a Lakeshore 330 temperature controller.

Device parameters such as carrier mobility, μ , on/off current ratio, and threshold voltage (V_{Th}) were estimated using the standard saturation regime current-voltage characteristics: $I_{DS} = \frac{\mu WC_O}{2L} (V_{GS} - V_{Th})^2$. I_{DS} is the drain-source current, C_O is the dielectric capacitance per unit area, and W

and L correspond to the channel width and length, respectively. L varied between 50 and 100 µm and W was either 0.5 mm or 1 mm.

III. RESULTS AND DISCUSSIONS

A. Charge transport models in disordered systems

We begin this section with a short description of the transport models in disordered systems. In comparison with inorganic semiconductors, organic semiconductors have (a) small carrier densities, (b) the Fermi level position depends on the background of unintentional dopants, (c) samples are depleted throughout their thickness, and (d) undoped samples are insulating-like. These differences result in a modification of transport characteristics in organic semiconductors compared to their inorganic counterpart. Several models have been proposed to describe charge transport in organic materials: variable range hopping,² delocalized charge transport,²⁶ multiple trapping and release,^{27,28} and other hybrid models.²⁹ As shown in Fig. 1(a), disordered systems are characterized by both localized and extended states. The concept of transport energy has been developed to describe hopping transport in band tails with purely exponential DOS. The DOS may be described by 30,31

$$g(E) = \frac{N_0}{E_0} \exp\left(-\frac{E}{E_0}\right),\tag{2}$$

where N₀ is the concentration of localized tail states and E₀ is the tailing parameter such that the E_F is thought to be deep in the gap at energies $E_F \ge E_0$. The localization energy, E, is measured positive from the mobility edge (E = 0) toward the gap center. There are three temperature regimes for the conductivity: (1) $k_BT \ge E_0$: conductivity is due to activation of carriers from the Fermi level into extended states; (2) Low temperature limit: Mott's law for variable range hopping is applicable, i.e., hopping of carriers between states in a narrow band near the Fermi level. The Mott behavior for conductivity in this temperature regime is given by $\sigma = \sigma_0 \exp(-T/T_0)^{1/4}$; (3) Intermediate temperature: conductivity may still be determined by variable range hopping, but the exponential growth of DOS results in a so-called transport energy.

The transport energy concept was introduced by Monroe in terms of a non-equilibrium energy relaxation problem where the electrons directly hop between localized bandtail states.³² Starting from the mobility edge, the electrons hop downward in energy. This relaxation process changes at some particular energy, Et, represented as the transport energy (TE). The hopping process near and below this energy resembles dispersive transport with E_t playing the same role as the mobility edge. The hopping rate of electrons between localized states may be described by Miller Abraham's formalism³³

$$v_{ij} = v_0 \exp\left(-2\frac{R_{ij}}{\alpha} - \frac{(E_i - E_j + |E_j - E_i|)}{k_B T}\right).$$
 (3)

In Eq. (3), v_{ij} is the rate for hop between an occupied site i and an empty state j separated by a distance R_{ij} ; α is the decay length of the wave function; and v_0 is the attempt-to-hop or attempt-to-escape frequency, typically of the order 10¹² s⁻¹. Since decreasing DOS makes it difficult for a charge carrier to find a neighbor at low energies, carriers in deep states move by thermal excitation to shallower states, while carriers in shallow states move by hopping to other shallow states.

Strictly, organic/polymeric semiconductors are characterized by a Gaussian DOS since the distribution of disordered potential leads to electron localization, which has a Gaussian distribution. The DOS is given by $g(E) = \frac{N_0}{\sqrt{\pi}E_0} \exp\left[-(E/E_0)^2\right]$, where E is measured from the distribution center (E = 0) and is positive for deeper energies.³¹ One can further formulate the Gaussian DOS in a standard form by replacing $E_0 = \sqrt{2}\sigma'$, where σ' the width of the Gaussian DOS is a measure of the energetic disorder. Figure 1(b) shows a comparison of the Gaussian DOS with an exponential one. The energy domain probed under most experimental conditions is such that the number of states as a function of energy is comparable for both Gaussian and exponential DOS. Although one can invoke the concept of TE with Gaussian DOS as well, an exact analytical form is not possible. One of the implications of the Gaussian DOS is that carriers have a finite mobility, which is given by

$$\mu = \mu_0 \exp\left[-\left(\frac{2\sigma'}{3k_{\rm B}T}\right)^2\right]. \tag{4}$$

Equation (4) follows from the zero field limit: $\mu = \mu_0 \exp$ $\left[-\left(\frac{T_0}{T}\right)^2\right]$, where μ_0 is the mobility of a disorder-free material at $T \to \infty$.³⁴ The characteristics temperature, T_0 , is related to the width of the Gaussian DOS by $k_BT_0 = 2\sigma'/3$. We shall see later that σ' is relatively small for transport through TIPS-pentacene FETs. Therefore, we can consider an exponential DOS. Furthermore, the temperature and field dependence (resembling Poole-Frenkel behavior) of carrier mobility in disordered polymers is often modeled as³³

$$\mu(T, E) = \mu_0 \exp\left\{-\left(\frac{2\sigma'}{3k_BT}\right)^2\right] \times \exp\left[C\left[\left(\frac{\sigma'}{k_BT}\right)^2 - \Sigma^2\right]E^{1/2}\right\},\tag{5}$$

where C is an empirical constant and Σ is a parameter that may be related to the Miller Abraham's formalism [Eq. (3)], denoting the local variations of the nearest-neighbor intersite distance.

B. Room temperature FET mobility as a function of the gate dielectric

In an FET architecture, the dielectric-semiconductor interface plays a large role in governing transport. Hence, the same semiconductor can display vastly varying carrier mobilities depending on the choice of the dielectric layer. For example, rubrene single crystal FETs have shown decreasing FET mobilities with increasing κ of the dielectric insulator due to polarization effects across the interface, a consequence of the Fröhlich polarons. The Fröhlich polarons reflect a long-range interaction between the charge carriers and the longitudinal optical phonons. It is these interactions at the interface that result in a renormalization of the transfer integral for the transport process and manifests itself as reduced charge carrier mobility when the dielectric constant of the gate insulator increases.

Several FET geometries, shown in Figs. 2(a)-2(c), utilizing TIPS-pentacene were fabricated. As discussed in Sec. II, the PVDF-TrFE films used were both unpoled and vertically poled. A recent work by Laudari et al.²³ shows that the FET properties may be greatly improved upon vertically poling the PVDF-TrFE layer. The architecture shown in Fig. 2(b) serves as a dual gate geometry, where one can use either the top gate insulator (CYTOP) or the bottom gate insulator with the same semiconducting film for transport measurements. Along with oxide dielectrics (SiO₂ or Al₂O₃), bilayer dielectrics (PVDF-TrFE/SiO₂) were also fabricated. These bilayer devices allow obtaining information on the Fröhlich polarons, as discussed in Ref. 24. The interface between the ferroelectric dielectric and TIPS-pentacene in bilayer devices is the same as shown in (a), except that the PVDF-TrFE layer is not an active ferroelectric since the SiO₂ layer is gated.

Figure 2(d) shows a clear trend of decreasing carrier mobility in TIPS-pentacene FETs with increasing κ of the gate insulator. Although PVP and SiO₂ have similar κ , it is not surprising that SiO₂ shows a slightly lower value of μ as oxide dielectrics are known to trap charges at the interface. PVDF-TrFE and Al₂O₃ dielectrics, which have the highest κ values at 300 K, show the lowest carrier mobility. Poling the

PVDF-TrFE (in the vertical direction) is seen to enhance μ by more than 3 times compared to the unpoled film. The carrier mobilities shown here are the average values of more than 10 devices. We will later see that the temperature dependence of μ for unpoled and poled PVDF-TrFE films in TIPS-pentacene FETs shows different trends.

C. Temperature-dependent FET mobility as a function of the gate dielectric

In this section, we look at two regions: the low temperature regime (100-220 K) and the high temperature regime (220-320 K). Unlike pentacene, TIPS-pentacene films are known to show cracks above 340 K; hence, we are limited to a temperature range up until room temperature. This also implies that one does not access the full range of κ values for PVDF-TrFE in the ferroelectric phase as the transition temperature is close to 390 K. Figure 3 shows the transfer curves at different temperatures for TIPS-pentacene utilizing CYTOP (which has the lowest value of κ) and Al₂O₃ with the highest value of κ , compared to the dielectrics used in this work. The carrier mobilities were extracted from the saturation region as described in Sec. II. Both of them clearly show an activated transport behavior. We can fit the data to a thermally activated hopping of charges from site to site within a disorder induced exponential distribution of states, as proposed by Monroe.³² In this model, the temperature dependence of μ is given by

$$\mu = \mu' \exp\left(-\frac{\Delta}{k_{\rm B}T}\right),\tag{6}$$

where Δ , the activation energy, is the energetic difference between the Fermi energy and the transport level, μ' is the mobility in the absence of any trap states, and k_B is the

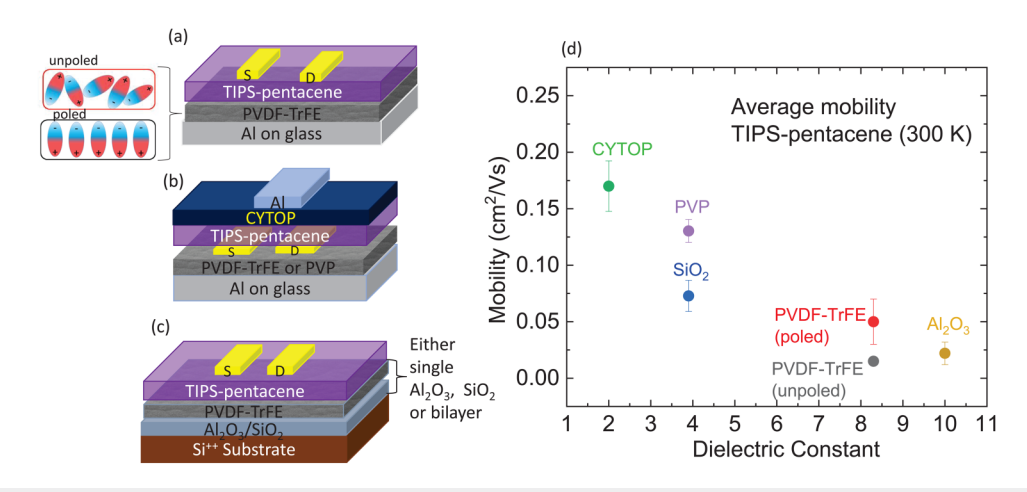


FIG. 2. Schematic of FET structures. (a) Bottom gate PVDF-TrFE, where the dielectric layer was either unpoled or poled; (b) dual FET with PVDF-TrFE or PVP as bottom gate and CYTOP as top gate; (c) bottom gate SiO₂ and a bilayer structure with SiO₂ and PDF-TrFE. (d) Average carrier mobility of TIPS-pentacene for different gate dielectrics.

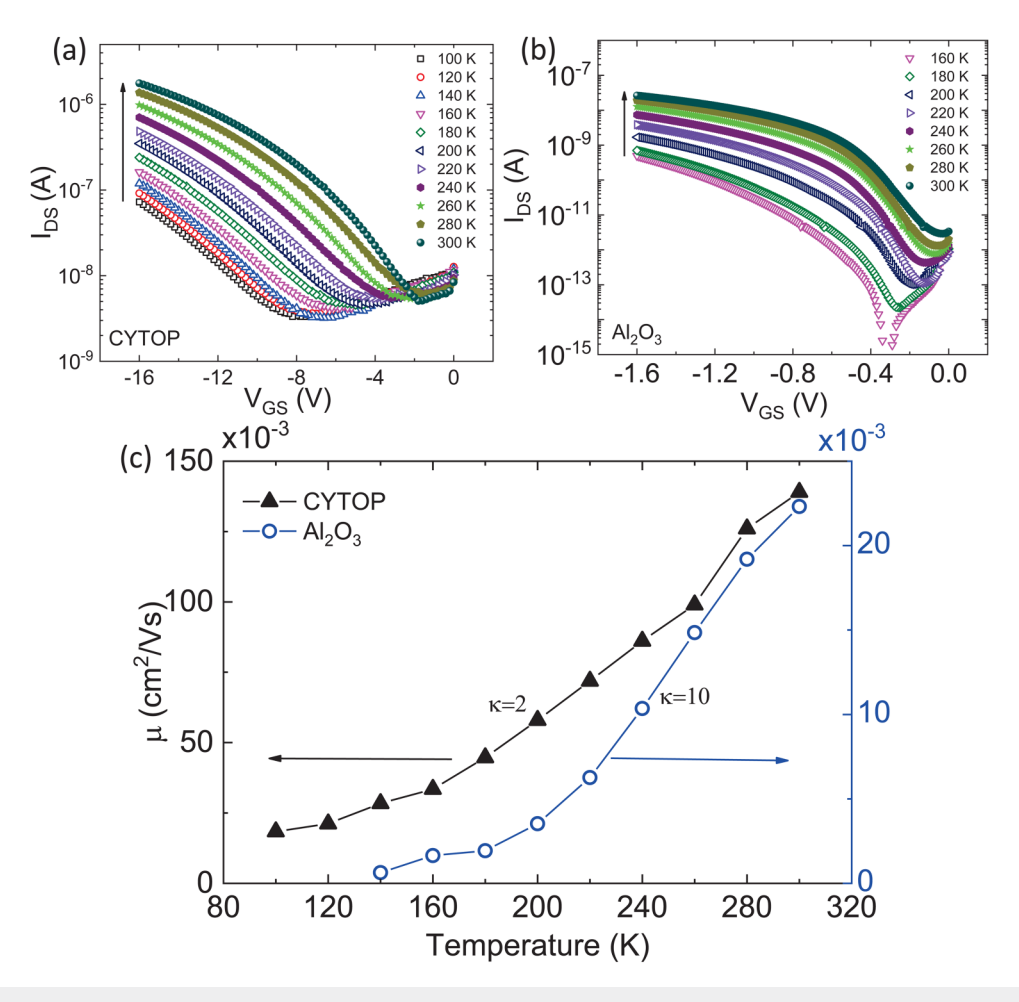


FIG. 3. Transconductance curves as a function of temperature from TIPS-pentacene FETs with CYTOP (a) and Al_2O_3 (b) dielectrics. (b) Extracted μ_{FET} as a function of temperature for CYTOP and Al_2O_3 dielectrics.

Boltzmann constant. Additionally, as the charge carrier density increases, the Fermi energy gets closer to the transport level, easing the transport of charges and thus decreasing Δ .

We use the temperature data from 100 to 220 K for some of the dielectrics to show the Arrhenius behavior of the carrier mobilities in TIPS-pentacene FETs (Fig. 4). We note that the Arrhenius behavior of several of the dielectrics used with TIPS-pentacene was shown in Ref. 21. The activation energy is seen to vary between 10 meV and 76 meV, the highest value being for Al_2O_3 with Δ = 76 meV, followed by PVDF-TrFE with Δ = 36 meV, SiO_2 with Δ = 27 meV, CYTOP with Δ = 23 meV, and bilayer PVDF-TrFE/ SiO_2 with Δ = 10 meV. This trend falls in place with the concept of a high dynamic coupling of the charge carriers with large values of κ . In this temperature range, κ for PVDF-TrFE varies between 3.9 and 4.5. Earlier, it has been observed that when PVDF-TrFE is utilized with pentacene where temperatures could be swept to 390 K (such that the highest value of

 $\kappa=25$ for PVDF-TrFE could be achieved), the activation energies are higher compared to the TIPS-pentacene/PVDF-TrFE results shown here. ²⁴ The PVDF-TrFE layer here is unpoled. Next, we present the differences between poled and unpoled PVDF-TrFE.

We now look at the temperature dependence of μ with PVDF-TrFE. Figure 5(a) shows μ as a function of temperature from both unpoled and vertically poled PVDF-TrFE. The data from unpoled PVDF-TrFE were presented in Ref. 21; however, in this work, we show a more exhaustive analysis. The mobilities were measured by sweeping the transfer curves at two different V_{DS} values at different temperatures for the unpoled device. Unlike unpoled PVDF-TrFE, where the carrier mobility decreases beyond 220 K, poled PVDF-TrFE shows a continuous increase in μ as a function of temperature. For the unpoled dielectric layer, $V_{DS} = -20 \, \text{V}$ shows a smaller activation energy for the Arrhenius plots compared to $V_{DS} = -10 \, \text{V}$, shown in Fig. 5(b) in the 100-220 K range. This is

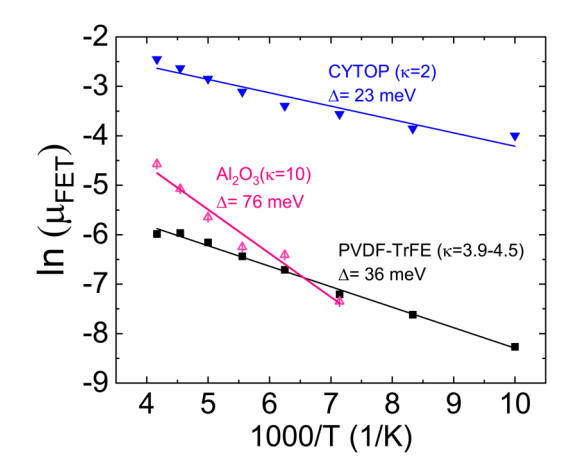


FIG. 4. Arrhenius plots of TIPS-pentacene FET mobilities for three different dielectric layers. The symbols are the experimental data and the lines are the fits.

expected for hopping transport that follows a Poole-Frenkel behavior [Eq. (5)].

Inorganic semiconductors which are described in terms of delocalized electronic bands show a negative coefficient of carrier mobility with temperature. Ordered organic semiconductors show a band-like behavior of the carrier mobility with $\mu \propto T^{-n}$, where n lies between 0.5 and 3. 36 In a typical band transport, the carriers are delocalized over several units, and the lattice phonons act as scattering sites. For these systems, there is almost no field dependence of μ . Thus, the absence of field-dependent mobility in organic transistors is a tell-tale of a band-like transport. For both voltage sweeps, the mobilities decrease beyond 240 K when

unpoled PVDF-TrFE is used. At lower temperatures, the mobility is clearly a function of the electric field, as expected from Eq. (5); however, beyond 240 K, both low and high field sweeps yield almost the same values of μ , which is a signature of band-like transport.

We mainly compare the trends observed in the FET mobilities in TIPS-pentacene FETs as a function of temperature and dielectrics, obtained from the saturation region as discussed in Sec. II. The different values of μ as a function of the dielectric layer (Fig. 2) clearly show that they are not intrinsic. Mobility measurements from FETs have received renewed attention. There have been recent discussions in the literature whether extracting carrier mobilities using the saturation region from FET transfer curves are appropriate. 37,38 Several works show that obtaining the mobility from the linear region of the FET transfer curve, which is given by $\mu_{\text{lin}} = \frac{\bar{L}}{WC_0V_{DS}} \frac{\partial I_{DS}}{\partial V_{CS}}$, is a better metric for reliable mobilities. However, the linear region is also affected to a greater extent by contact resistance compared to the saturation region, especially for small channel length devices.³⁹ A recent molecular-level FET device simulation shows that as long as the energetic disorder of the semiconductor is lower than $2k_BT$ (50 meV), the bulk mobility is similar to μ_{sat} and μ_{lin} ; hence, μ_{sat} may be applied for the analysis. 40 We estimate the energetic disorder (σ') by fitting the temperature-dependent μ_{FFT} data of unpoled PVDF-TrFE using Eq. (4), as shown in Fig. 6. In the temperature range where a true hopping transport is observed (from 100 to 220 K), the sweeps at two different values of V_{DS} yield σ' to be well below $2k_BT$, and, thus, one may justify extracting the carrier mobilities for TIPS-pentacene FETs from the saturation region of the transfer curves. We further fit the high temperature region where a band-like transport is observed with $\mu \propto T^{-n}$; n is found to be 2.7, similar to values observed in ordered organic semiconductors.

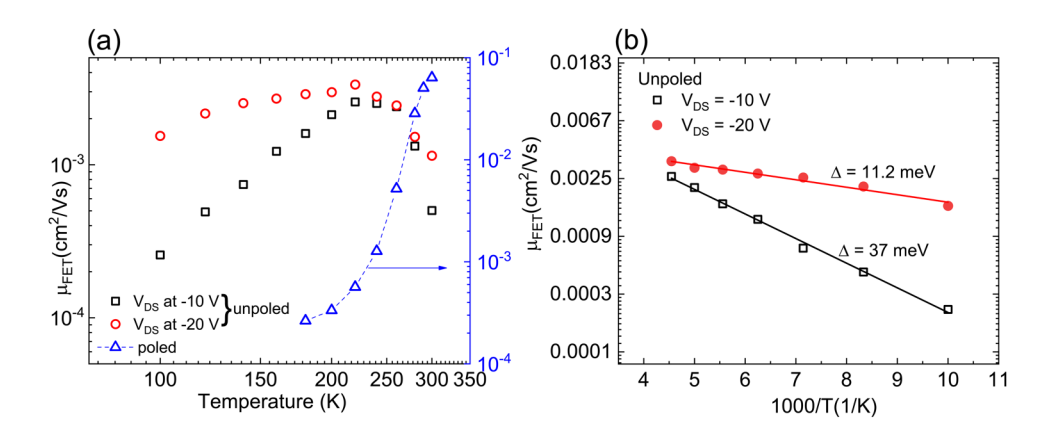


FIG. 5. (a) TIPS-pentacene FET mobility as a function of temperature at two different V_{DS} values for unpoled PVDF-TrFE. The blue triangles are the FET mobility from a TIPS-pentacene FET where the PVDF-TrFE dielectric layer was vertically poled. (b) Arrhenius plots of TIPS-pentacene FET mobilities shown in (a) in the temperature range of 100-220 K for unpoled PVDF-TrFE. The symbols are the experimental data and the lines are the fits.

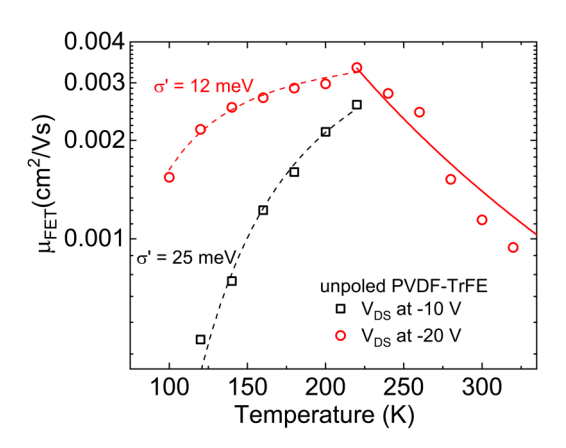


FIG. 6. Fits to the experimental TIPS-pentance μ_{FET} data using unpoled PVDF-TrFE as the dielectric. The temperature range between 100 and 220 K is fit with Eq. (4). The high temperature range for the sweep at V_{DS} at -20 V has been fit with $\mu \propto T^{-n}$.

IV. DISCUSSION

The trend in carrier mobilities as a function of temperature with varying dielectric films in TIPS-pentacene FETs is similar for all dielectrics except for unpoled PVDF-TrFE, which shows a negative coefficient of $d\mu/dT$ above 220 K. In a prior work, the bulk mobility of TIPS-pentacene was estimated from a two terminal device. The current-voltage characteristics of TIPS-pentacene diodes show a space-charge-limited conduction (SCLC) for discrete trap states, suggesting that charge injection and transport occurs through regions of ordering in the semiconductor. Such an SCLC shows four distinct regions in the current-voltage characteristics (log-log plot). Using the trap-free SCLC region, the bulk mobility can be directly extracted. It was observed that

the bulk mobility in TIPS-pentacene shows a negative $d\mu/dT$ beyond 180 K. 21

In order to understand the differences between unpoled PVDF-TrFE and its vertically poled counterpart, the trapped charge density (N_{trap}^{max}) was estimated from the subthreshold swing of the FET characteristics. $N_{trap}^{max} \approx \left[\frac{q \text{Slog(e)}}{k_B T} - 1\right] \frac{C_o}{q}$, where q is the elementary charge and C_o is the gate capacitance per unit area. The subthreshold swing, S, is given by $S = \left[\frac{d\log(I_{ds})}{dV_{e}}\right]^{-1}$. Usually, this method results in an estimate of the maximum trapped charge. Figure 7(a) plots N_{trap}^{max} for unpoled (swept at two different values of V_{DS}) and poled PVDF-TrFE FETs. Above 200 K, for which the poled FET was measured, the trap density is seen to be an order of magnitude higher for the poled FET compared to the unpoled device. At temperatures below 250 K, we find the carrier mobility of the poled PVDF-TrFE FET is lower than the unpoled FET; however, this trend changes beyond 250 K. At 300 K, the carrier mobility in the poled FET is almost two orders of magnitude higher compared to the unpoled sample, although the trap density does not alter. The nature of transport with poled PVDF-TrFE is similar to other nonferroelectric dielectrics. These observations suggest that the trapped charge density is not the only factor that governs carrier mobility. The energy fluctuations due to the randomly oriented dipoles that are present locally in the unpoled PVDF-TrFE films are responsible for band-like transport as well as lower values of μ compared to poled PVDF-TrFE, seen above temperatures of 200 K. The difference in transport does not stem from contact resistance issues. For channel lengths lower than $10 \,\mu\text{m}$, the transistor performance is usually contact limited. 41 The contact resistance of FETs used in this work is minimal as the channel lengths are relatively large (50-100 μ m). The contact resistance was at least two orders of magnitude smaller than the channel resistance, and the difference between the poled and unpoled FETs was minimal, similar to what was estimated in Ref. 23.

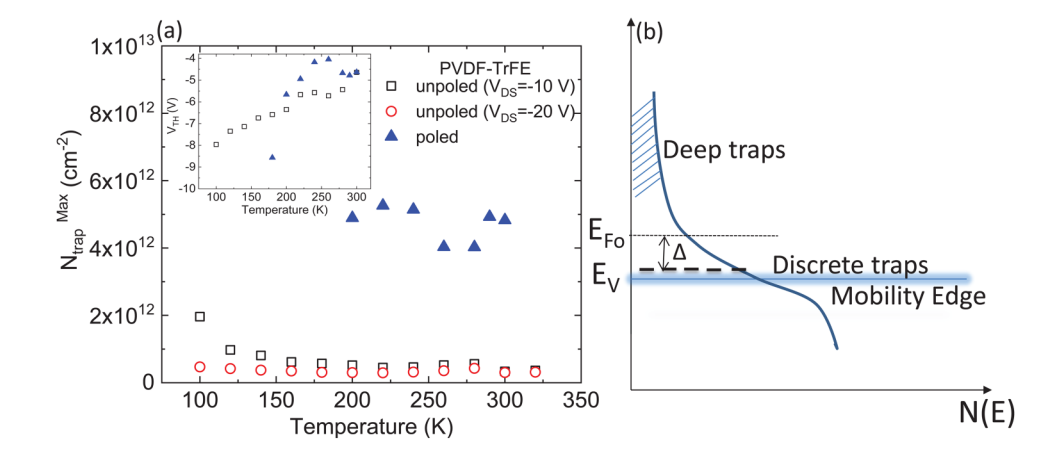


FIG. 7. (a) The trapped charge density as a function of temperature for TIPS-pentacene FETs using unpoled and vertically poled PVDF-TrFE. The inset shows the threshold voltage as a function of temperature for the poled and unpoled devices. (b) Schematic of the density of trapped carriers as a function of Fermi energy.

As expected, the threshold voltage decreases with the increase in temperature. Such a behavior is seen for hopping transport in FETs. We observe this trend as a shift of the transfer curves with temperature (Fig. 3). In order to understand the differences in the poled versus the unpoled FETs, we plot V_{Th} as a function of temperature in the inset of Fig. 7(a). The changes in V_{Th} are higher for the poled sample compared to the unpoled sample. It is worth noting that for the unpoled sample, in the temperature range where bandlike transport is observed, there is hardly any change in V_{Th}. This is again suggestive of the differences in the nature of transport, below and above 220 K, for the unpoled sample.

The bulk transport in TIPS-pentacene clearly shows the presence of discrete traps, schematically represented in Fig. 7(b). These are shallow traps, so one would expect them to have energies close to the mobility edge. We note that the analytical expression derived for shallow traps is valid as long as the Fermi energy is below the trap energy.⁴² Assuming exponentially increasing tail states, the Fermi energy (E_{FO}) movement is well below the deep trap states, within the tail states and the mobility edge. Using the concept of mobility edge, one expects the density of carriers excited to the isoelectronic transport band to follow: $n_{band} = N_b \exp(E_F/k_BT)$, where N_b is the effective state density of the transport band. One can similarly write down an expression for the trapped carriers $(n_{trapped})$. For hopping transport, we expect $n_{\text{trapped}} \gg n_{\text{band}}$. However, with the presence of discrete traps, it is conceivable that polarization fluctuation, inherent to unpoled PVDF-TrFE, reduces the trap depth due to screening. This process may facilitate transport through discrete traps, which manifests itself as a band-like transport. Thus, there seems to be a competition between the tail states and discrete trap levels in TIPS-pentacene, and at temperatures above 220 K, the polarization fluctuation in PVDF-TrFE is responsible for bringing the Fermi energy closer to the mobility edge. Other semicrystalline conducting polymers also show discrete traps states in bulk transport⁴³ and may thus display such band-like behavior in FET transport.

V. CONCLUSIONS

Temperature dependent transport properties were measured from TIPS-pentacene FETs using a variety of dielectrics with varying κ . The transport measurements were tuned until \sim 320 K, where the κ for PVDF-TrFE is just above 8.0, at par with Al₂O₃. The carrier mobility shows an activated transport throughout the temperature range when Al₂O₃ is used in contrast to unpoled PVDF-TrFE, which shows a band-like transport with $d\mu/dT < 0$ above 220 K. By fitting the high temperature regime of unpoled PVDF-TrFE devices to $\mu \propto T^{-n}$, n was found to be 2.7, similar to values obtained for ordered organic semiconductors. All other non-ferroelectric dielectrics and poled PVDF-TrFE (where the dipoles are prealigned) show an activated transport similar to Al₂O₃, suggesting that the reduced mobility with unpoled PVDF-TrFE is not just due to the long-range polaron coupling but rather

due to its inherent polarization fluctuation in conjunction with the nature of discrete trap-states in TIPS-pentacene.

ACKNOWLEDGMENTS

We acknowledge the support of this work through the National Science Foundation (NSF) under Grant No. ECCS-1707588. We thank Shubhra Gangopadhyay for providing us with the Al₂O₃ substrates.

REFERENCES

- ¹N. F. Mott and E. A. Davis, Electronic Processes in Non-crystalline Materials (Clarendon Press; Oxford University Press, Oxford, New York,
- ²M. C. J. M. Vissenberg and M. Matters, Phys. Rev. B 57, 12964 (1998).
- ³H. Bässler, Phys. Status Solidi B **175**, 15 (1993).
- ⁴H. Houili, J. D. Picon, L. Zuppiroli, and M. N. Bussac, J. Appl. Phys. 100, 023702 (2006).
- ⁵S. J. Konezny, M. N. Bussac, and L. Zuppiroli, Phys. Rev. B **81**, 045313 (2010). ⁶I. N. Hulea, S. Fratini, H. Xie, C. L. Mulder, N. N. Iossad, G. Rastelli, S. Ciuchi, and A. F. Morpurgo, Nat. Mater. 5, 982 (2006).
- ⁷M. V. Fischetti, D. A. Neumayer, and E. A. Cartier, J. Appl. Phys. 90, 4587
- ⁸M. V. Fischetti, J. Appl. Phys. **89**, 1232 (2001).
- ⁹P. Servati, A. Nathan, and G. A. J. Amaratunga, Phys. Rev. B 74, 245210
- 10S. P. Senanayak, A. Z. Ashar, C. Kanimozhi, S. Patil, and K. S. Narayan, Phys. Rev. B 91, 115302 (2015).
- ¹¹S. Fratini, D. Mayou, and S. Ciuchi, Adv. Funct. Mater. 26, 2292 (2016).
- ¹²S. Stafström, Chem. Soc. Rev. **39**, 2484 (2010).
- 13Y. Mei, P. J. Diemer, M. R. Niazi, R. K. Hallani, K. Jarolimek, C. S. Day, C. Risko, J. E. Anthony, A. Amassian, and O. D. Jurchescu, Proc. Natl. Acad. Sci. 114, E6739 (2017).
- ¹⁴J. Hoffman, X. Pan, J. W. Reiner, F. J. Walker, J. P. Han, C. H. Ahn, and T. P. Ma, Adv. Mater. 22, 2957 (2010).
- ¹⁵R. C. G. Naber, C. Tanase, P. W. M. Blom, G. H. Gelinck, A. W. Marsman, F. J. Touwslager, S. Setayesh, D. M. De Leeuw, Nat. Mater. 4, 243 (2005).
- ¹⁶J.-H. Lee, H.-J. Yoon, T. Y. Kim, M. K. Gupta, J. H. Lee, W. Seung, H. Ryu, and S.-W. Kim, Adv. Funct. Mater. 25, 3203 (2015).
- ¹⁷J. J. Brondijk, K. Asadi, P. W. M. Blom, and D. M. De Leeuw, J. Polym. Sci. B Polym. Phys. 50, 47 (2012).
- ¹⁸A. J. Lovinger, Science **220**, 1115 (1983).
- ¹⁹T. Furukawa, IEEE Trans. Electr. Insul. **24**, 375 (1989).
- ²⁰S. P. Senanayak, S. Guha, and K. S. Narayan, Phys. Rev. B **85**, 115311 (2012).
- ²¹A. Laudari and S. Guha, Phys. Rev. Appl. **6**, 044007 (2016).
- ²²T. Sakanoue and H. Sirringhaus, Nat. Mater. 9, 736 (2010).
- ²³A. Laudari, A. R. Mazza, A. Daykin, S. Khanra, K. Ghosh, F. Cummings, T. Muller, P. Miceli, and S. Guha, Phys. Rev. Appl. 10, 014011 (2018).
- ²⁴A. Laudari and S. Guha, J. Appl. Phys. **117**, 105501 (2015).
- ²⁵A. Laudari, S. Gangopadhyay, and S. Guha, MRS Adv. **2**, 2951 (2017).
- ²⁶S. E. Koh, B. Delley, J. E. Medvedeva, A. Facchetti, A. J. Freeman, T. J. Marks, and M. A. Ratner, J. Phys. Chem. B 110, 24361 (2006).
- ²⁷R. J. Chesterfield, J. C. McKeen, C. R. Newman, C. D. Frisbie, P. C. Ewbank, K. R. Mann, and L. L. Miller, J. Appl. Phys. 95, 6396 (2004).
- ²⁸R. J. Chesterfield, J. C. McKeen, C. R. Newman, P. C. Ewbank, D. A. da Silva Filho, J. L. Brédas, L. L. Miller, K. R. Mann, and C. D. Frisbie, J. Phys. Chem. B 108, 19281 (2004).
- ²⁹K. Waragai, H. Akimichi, S. Hotta, H. Kano, and H. Sakaki, Phys. Rev. B 52, 1786 (1995).
- ³⁰S. Marianer and B. I. Shklovskii, Phys. Rev. B **46**, 13100 (1992).
- 31 S. D. Baranovskii, T. Faber, F. Hensel, and P. Thomas, J. Phys. Condens. Matter 9, 2699 (1997).
- 32D. Monroe, Phys. Rev. Lett. 54, 146 (1985)
- 33A. Miller and E. Abrahams, Phys. Rev. 120, 745 (1960).

- 34P. M. Borsenberger, J. Appl. Phys. 68, 6263 (1990).
- ³⁵P. M. Borsenberger, L. Pautmeier, and H. Bässler, J. Chem. Phys. **94**, 5447 (1991).
- 36V. Coropceanu, J. Cornil, D. A. da Silva Filho, Y. Olivier, R. Silbey, and J. L. Brédas, Chem. Rev. 107, 926 (2007).
- ³⁷H. H. Choi, K. Cho, C. D. Frisbie, H. Sirringhaus, and V. Podzorov, Nat. Mater. 17, 2 (2018).
- ³⁸Y. Xu, H. Sun, A. Liu, H. Zhu, B. Li, T. Minari, F. Balestra, G. Ghibaudo, and Y.-Y. Noh, Adv. Funct. Mater. **28**, 1803907 (2018).
- ³⁹Z. A. Lamport, H. F. Haneef, S. Anand, M. Waldrip, and O. D. Jurchescu, J. Appl. Phys. **124**, 071101 (2018).
- ⁴⁰H. Li, N. Tessler, and J. L. Brédas, Adv. Funct. Mater. **28**, 1803096 (2018).
- ⁴¹D. J. Gundlach, L. Zhou, J. A. Nichols, T. N. Jackson, P. V. Necliudov, and M. S. Shur, J. Appl. Phys. **100**, 024509 (2006).
- ⁴²M. A. Lampert and P. Mark, Current Injection in Solids (Academic, New York, 1970).
- ⁴³M. Arif, M. Yun, S. Gangopadhyay, K. Ghosh, L. Fadiga, F. Galbrecht, U. Scherf, and S. Guha, Phys. Rev. B 75, 195202 (2007).